Available online at www.sciencedirect.com
ScienceDirect
International Journal of Multiphase Flow 32 (2006) 1234–1253
International Journal of Multiphase Flow
www.elsevier.com/locate/ijmulflow

Stochastic modeling of particle diffusion in a turbulent boundary layer

T.L. Bocksell [a], E. Loth [b,*]

[a] Pratt and Whitney, 400 Main Street, MS 184-42, East Hartford, CT 06108, USA
[b] Department of Aerospace Engineering, University of Illinois at Urbana-Champaign, 306 Talbot Laboratory, 104 South Wright Street, Urbana, IL 61801-2935, USA

Received 8 November 2004; received in revised form 24 May 2006

Abstract

Several Continuous Random Walk (CRW) models were constructed to predict turbulent particle diffusion based on Eulerian statistics that can be obtained with Reynolds-Averaged Navier Stokes (RANS) solutions. The test conditions included a wide range of particle inertias (Stokes numbers) with a near-wall injection ($y^+ = 4$) in a turbulent boundary layer that is strongly anisotropic and inhomogeneous. To assess the performance of the models, the CRW results were compared to particle diffusion statistics gathered from a Direct Numerical Simulation (DNS). In particular, comparisons were made with transverse concentration profiles, root-mean-square of particle trajectory coordinates, and mean transverse particle velocity away from the wall.

The results showed that accurate simulation required a modified (non-dimensionalized) Markov chain to handle the large gradients in turbulence near the wall as shown by simulations with fluid-tracer particles. For finite-inertia particles, an incremental drift correction for the Markov chain developed herein to account for Stokes number effects was critical to avoiding non-physical particle collection in low-turbulence regions. In both cases, inclusion of anisotropy in the turbulence model was found to be important, but the influence of off-diagonal terms was found to be weak. The results were generally good, especially for long-time and large inertia particles.
© 2006 Elsevier Ltd. All rights reserved.

Keywords: Two-phase flow; Lagrangian; Markov chain; Turbulent particle diffusion; Direct numerical simulation; Turbulent boundary layer

1. Introduction

1.1. Overview of turbulent diffusion of particles in boundary layers

Understanding the dynamics of a multi-phase system has long been an issue of scientific and engineering interest. Of particular interest to this study is the numerical simulation of particle diffusion due to turbulence

* Corresponding author. Tel.: +1 217 244 5581.
E-mail address: loth@uiuc.edu (E. Loth).

0301-9322/$ - see front matter © 2006 Elsevier Ltd. All rights reserved.
doi:10.1016/j.ijmultiphaseflow.2006.05.013

in the continuous phase, where the density of the particles is assumed to be much greater than the density of the surrounding fluid. Let us first consider some relevant non-dimensional diffusion parameters for turbulence that is isotropic and homogeneous: the particle integral-scale Stokes number (St_Λ) is the ratio of particle relaxation time (τ_p) to a local turbulent integral time-scale (τ_Λ); the wall-based Stokes number (St^+) is the ratio of the particle relaxation time to the wall based time-scale (v_f/u_τ^2); the drift parameter (γ) is the ratio of particle terminal velocity (V_{term}) to the root-mean-square of the fluid fluctuation velocities ($u'_{f,\,rms}$); and the particle Reynolds number ($Re_{p,\,term}$) based on the particle terminal velocity:

$$St_\Lambda = \frac{\tau_p}{\tau_\Lambda}, \quad St^+ = \frac{\tau_p u_\tau^2}{v_f}, \quad \gamma = \frac{V_{\,term}}{u'_{f,\,rms}}, \quad Re_{p,term} = \frac{V_{term} d_p}{v_f}, \tag{1}$$

where d_p is the particle diameter, v_f is the fluid kinematic viscosity, ρ_f is the fluid density, ρ_p is the particle density, and

$$V_{term} = \frac{\tau_p}{g} = \frac{\rho_p d_p^2}{18\mu_f}. \tag{2}$$

For homogenous, isotropic turbulence (HIsT), Crowe et al. (1988) identified three distinct regimes of particle diffusion based on the particle Stokes number. For very small Stokes number particles ($St_\Lambda \ll 1$), the particles have a very short relaxation time and follow the fluid motion closely and thus have similar mass diffusion as that of the continuous-phase. For very large Stokes number particles ($St_\Lambda \gg 1$), the particles have a very long relaxation time and the turbulence only has a limited effect on the trajectories because the eddy-particle interaction time is not long enough to overcome the large inertia of the particles and therefore particle mass diffusion is significantly less than that of the continuous phase. For intermediate Stokes number particles, ($St_\Lambda \approx 1$), the particles do not follow the fluid exactly, however there is a noticeable effect on the particle velocity and trajectory due to the turbulent eddies. In general, this leads to a monotonic reduction in turbulent diffusion as particle Stokes number increases.

For inhomogeneous turbulence (where the average turbulent statistics have significant spatial variations), the physics is more complex. In particular, the gradient in the turbulent kinetic energy can cause changes in particle diffusion. Kaftori et al. (1995) experimentally studied the motion of particles near the wall of a turbulent boundary layer and noted that particles with wall-based Stokes numbers of order unity ($St^+ \approx 1$) yielded high concentrations near the wall and was described as ''wall-peaking''. Young and Leeming (1997) noted that this phenomenon is due to ''turbophoresis'' (a convective drift of particles down gradients of mean-square fluctuating velocity) and could be qualitatively described with an Eulerian model as a function of a wall-based Stokes number (St^+). These gradients have also been found to be important for particle diffusion in pipe flows and shear layers such that an accurate methodology to predict this behavior is needed for multi-phase engineering systems.

1.2. Methodologies for simulation of particle diffusion

Numerical simulation of a two-phase flow system can either be accomplished by treating the particles in an Eulerian or a Lagrangian frame, each has specific advantages and disadvantages as noted by Loth (2000). In this research, the Lagrangian approach is utilized because it allows for the crossing trajectories effect and particle–wall reflection phenomena. The latter is especially important herein because wall collisions can be a major factor in the resulting particle distribution for the turbulent boundary layer simulations.

For the treatment of the continuous fluid, it is ideal to describe all the spatial and temporal scales down to the Kolmogorov scales for turbulent flows, and this approach is termed Direct Numerical Simulation (DNS). However, it is not practical to obtain this resolution for many engineering systems since the computational resources required rapidly increases with Reynolds number. A common approach is to instead predict only the time-averaged velocity and turbulence properties using a Reynolds Averaged Navier Stokes (RANS) approach, which requires much less computational resources than DNS. To transform such statistics into instantaneous fluid fluctuation velocities seen by the particles in a Lagrangian frame, a Continuous Random Walk (CRW) model can be used along with a statistically large number of particles to obtain mean particle diffusion. This stochastic model correlates the velocity fluctuations from the previous time-step through a

Markov chain (based on a Langevin equation), with the inclusion of a random variable. These types of Markov chains are computational fast to evaluate and simple to program. These chains can also be used to model the sub-grid stress fluctuations for Lagrangian particle trajectories for Large Eddy Simulation as indicated by Loth (2000).

Markov chains are based on Langevin equations, such as

$$\frac{\mathrm{d}u}{\mathrm{d}t} = -\alpha u(t) + \lambda\xi(t), \tag{3}$$

where the continuous random variable, $\xi(t)$, can be specified to have a Gaussian distribution with a variance of unity. The Markov chain for a homogeneous and isotropic flow developed Legg and Raupach (1982), based on (3), is

$$u(t+\Delta t) = u(t)\exp\left(\frac{-\Delta t}{\tau_\mathrm{L}}\right) + \left[1-\exp\left(\frac{-2\Delta t}{\tau_\mathrm{L}}\right)\right]^{1/2}\sigma(t)\xi(t). \tag{4}$$

However, Wilson et al. (1981) suggested using a normalized Langevin equation of the form

$$\frac{\mathrm{d}}{\mathrm{d}t}\left(\frac{u}{\sigma}\right) = -\alpha\left(\frac{u}{\sigma}\right) + \lambda\xi(t) \tag{5}$$

to allow for inhomogeneous turbulence. Iliopoulos and Hanratty (1999) utilized this normalized Langevin equation in their analysis of near-wall fluid-tracer diffusion and the resulting normalized Markov chain is

$$u(t+\Delta t) = \exp\left(\frac{-\Delta t}{\tau_\mathrm{L}}\right)u(t)\frac{\sigma(t+\Delta t)}{\sigma(t)} + \left[1-\exp\left(\frac{-2\Delta t}{\tau_\mathrm{L}}\right)\right]^{1/2}\sigma(t+\Delta t)\xi(t). \tag{6}$$

A key issue in using a Markov chain in combination with inhomogeneous turbulence is that the inhomogeneity of the turbulence needs to be included in the Markov chain or non-physical, numerical particle diffusion occurs. MacInnes and Bracco (1992) investigated the performance of a CRW model, similar to the one of Legg and Raupach (1982), in 2-D inhomogeneous turbulent flows of a turbulent mixing layer and axisymmetric jet, and determined that a drift correction of

$$\delta\overline{v_\mathrm{f}'} = \tau_\Lambda\left[1-\exp\left(\frac{-\Delta t}{\tau_\Lambda}\right)\right]\frac{\partial}{\partial y}\left(v_\mathrm{f}'v_\mathrm{f}'\right) \tag{7}$$

should be included in the Markov chain. According to Bocksell and Loth (2001), this can also be expressed as

$$\delta\overline{u_{\mathrm{f}_i}'} = \Delta t\left(\overline{\frac{\mathrm{D}u_{\mathrm{f}_i}'}{\mathrm{D}t}}\right) = \Delta t\left(\overline{u_{\mathrm{f}_j}'\frac{\partial u_{\mathrm{f}_i}'}{\partial x_j}}\right), \tag{8}$$

which is equivalent to (7) to first order. Not including this drift correction, errors of up to 500% for the particle number concentration were found (while inclusion reduced the error to around 10%).

Iliopoulos and Hanratty (1999) investigated the turbulent dispersion of fluid-tracers released at $y^+ = 40$ in a turbulent channel flow and used the modified Langevin equation (including a drift correction) to obtain velocity fluctuations along a particle trajectory. The random walk model was compared to DNS diffusion results for these zero-inertia (fluid-tracer) particles, and in general it was found that the performance was reasonable. More recently, Mito and Hanratty (2005), investigated the effect of gravitational settling on particle concentration profiles in a channel flow. The modified Lagrangian equation was similarly utilized for a range of finite inertial particles, however the drift correction was based on the tracer particle formulation and did not include finite inertia effects.

This research addresses the effect of particle inertia on the drift correction where no previous studies (to the authors knowledge) have derived the drift correction for finite-inertia particles. In addition, no CRW simulations have evaluated random-walk model performance with a near-wall release of particles (such as in the viscous sub-layer) where the anisotropic and inhomogeneous effects are the strongest. The current study seeks to address these two issues since they can be important for finite-size particles injected or ablated near the surface of a turbulent boundary layer or in other flows that are strongly inhomogeneous. In addition, a second

objective is to investigate the level of flow detail needed for successful particle diffusion prediction. Therefore, Markov chains will be based on increasing levels of sophistication for the Eulerian mean flow statistics: isotropic turbulence, anisotropic turbulence for the three directions only (neglecting off-diagonal terms), and anisotropic turbulence with the full stress-tensor (including off-diagonal terms).

2. Methodology

2.1. DNS solution and RANS-like statistics

The continuous phase solution for the turbulent boundary layer was obtained from DNS of the incompressible Navier–Stokes equations, assuming the particle concentration is dilute (does not affect the carrier phase) and negligible particle–particle interactions. The DNS code was developed by Spalart and Watmuff (1993) to simulate a three-dimensional, spatially developing boundary layer with no streamwise pressure gradient. The method is spectrally accurate in the three spatial directions and second-order accurate in time. The solution domain is semi-infinite over a flat, smooth surface with $0 \leqslant x \leqslant \Lambda_x$, $-\infty \leqslant z \leqslant \infty$, and $0 \leqslant y \leqslant \infty$, where x, z, and y represent the streamwise, spanwise, and transverse directions and where Λ_x is the streamwise domain length.

The Reynolds number of a turbulent boundary layer can be based on the large-scale parameters ($Re_\delta = U_\infty \delta / \nu_f$), where δ is the boundary layer thickness and U_∞ is the free-stream velocity. For the present Reynolds boundary number ($Re_\delta = 4500$), grid-independent results were obtained for a domain discretized by 256 nodes in the stream direction, 96 in the span direction, and 55 in the transverse direction for a total of 1,351,680 nodes in the three-dimensional mesh. Spatial evolution aspects and time integration details are given by Bocksell (2004) and Dorgan (2003).

Eulerian time-averaged/spanwise-averaged statistics of the fluid properties are shown in Fig. 1 for transverse profiles at $x = \Lambda_x/3$ of the mean velocity (in wall units) as well as turbulent kinetic energy and velocity fluctuations (normalized by u_τ^2). For the mean velocity profile, there is evidence of the viscous sublayer below $y^+ \approx 20$ and a transition to a logarithmic curve is seen by $y^+ \approx 50$. The boundary layer edge is located at roughly $y^+ \approx 270$ (or $Re_\tau = 270$ where Re_τ is the Reynolds number based on δ and u_τ) and the common "law of the wall" curves are included for the purpose of comparing the data to high Reynolds number boundary layers. The peak values for k and $v'_{f,\mathrm{rms}}$ results are similar in magnitude to experimental results of Klebanov reported by Hinze (1975) at $Re_\tau = 2800$, though at somewhat larger y^+ locations. These Eulerian statistics, along with the full Reynolds-stress tensor and the turbulent dissipation (ε), were used to construct a typical RANS-like turbulent boundary layer flow solution by Bocksell (2004).

Based on HisT flow, Hinze (1975) utilized asymptotic analysis and dimensional arguments that led to approximations for the Lagrangian turbulent time and length scales as functions of the turbulent kinetic energy and dissipation. However, as noted by Bocksell and Loth (2001), the Lagrangian turbulent length and time scales (τ_Λ and Λ) in a boundary layer are not approximated sufficiently by the HIsT assumption and instead depend on distance from the wall (y^+). Therefore, the DNS was utilized to obtain these values across the boundary layer. To obtain this information, 4000 fluid-tracer particles (scalars) were released at 45 locations in the wall-normal direction within the boundary layer. The following Lagrangian autocorrelations were evaluated at every time step by ensemble-averaging over all the fluid-tracer particle paths,

$$R_{uu}(\tau) = \frac{\overline{u'_f(t)u'_f(t+\tau)}}{\overline{u'_f(t)u'_f(t)}}, \quad R_{vv}(\tau) = \frac{\overline{v'_f(t)v'_f(t+\tau)}}{\overline{v'_f(t)v'_f(t)}}, \quad \text{and} \quad R_{ww}(\tau) = \frac{\overline{w'_f(t)w'_f(t+\tau)}}{\overline{w'_f(t)w'_f(t)}}. \tag{9}$$

With these autocorrelations, τ_{Λ_i} is obtained as a function of y-release point from

$$\tau_{\Lambda_u} = \int_0^T R_{uu}(\tau)\,\mathrm{d}\tau, \quad \tau_{\Lambda_v} = \int_0^T R_{vv}(\tau)\,\mathrm{d}\tau, \quad \text{and} \quad \tau_{\Lambda_w} = \int_0^T R_{ww}(\tau)\,\mathrm{d}\tau, \tag{10}$$

such that T is many times larger than the integral turbulent time scale. These time scales along with the root-mean-square of the turbulent fluctuations are used to compute the anisotropic integral turbulent length scale as

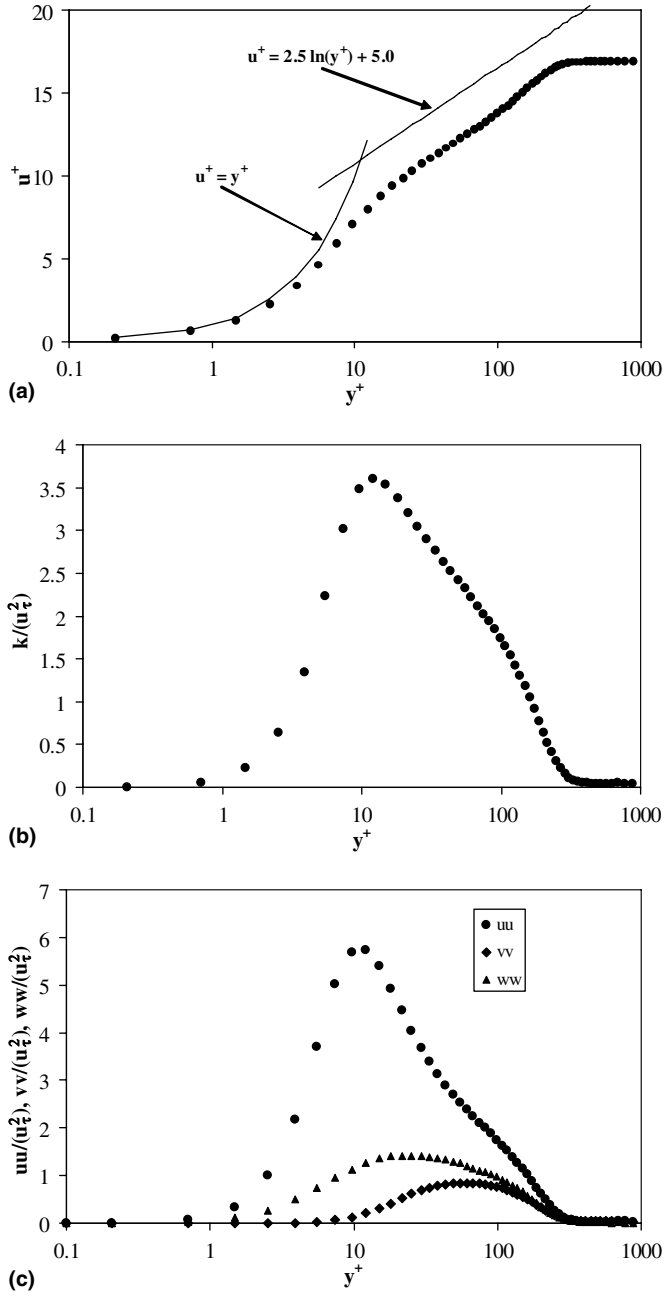

Fig. 1. DNS flow statistics at the particle injection plane, in wall units: (a) mean velocity profile, (b) turbulent kinetic energy profile, and (c) turbulent auto-correlation profiles.

$$\Lambda_i = C_\Lambda u'_{\mathrm{rms}_j} \tau_{\Lambda_i} \delta_{ij}. \tag{11}$$

Thus both Λ_i and τ_{Λ_i} were obtained as functions of distance from the wall for the turbulent boundary layer (as shown in Fig. 2) and were then used as a look-up table for the CRW model. Note that the estimated Lagrangian time scale of Kallio and Reeks (1989) for a turbulent boundary layer shows a very similar behavior to the DNS obtained time-scales, indicating that the length and time scales can be reasonably obtained from Eulerian statistics.

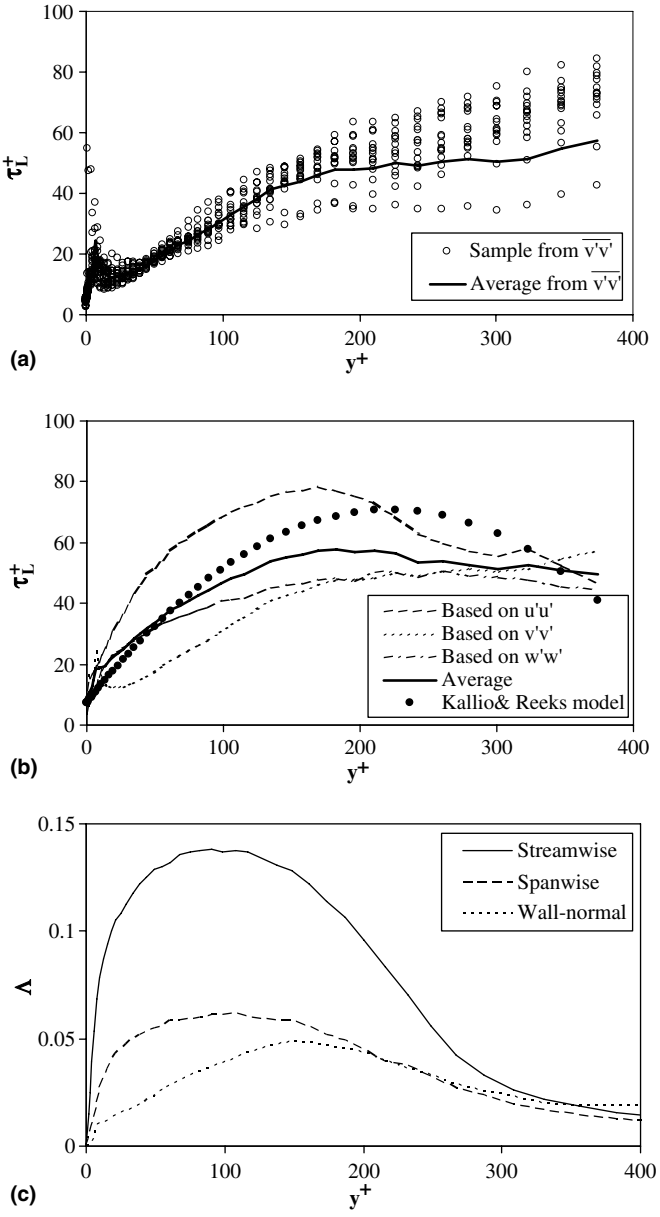

Fig. 2. (a) Lagrangian fluid time-scale profiles from DNS, (b) Lagrangian fluid time-scale component and average value profiles from DNS, and (c) Lagrangian fluid length-scale profiles from DNS.

2.2. Particle equation of motion

The particle equation of motion for both the DNS and CRW simulations is

$$m_{\mathrm{p}} \frac{\mathrm{d}u_{\mathrm{p}_i}}{\mathrm{d}t} = 3\pi\mu_{\mathrm{f}} d_{\mathrm{p}} (u_{\mathrm{f}_i} - u_{\mathrm{p}_i}) + m_{\mathrm{p}} g_i, \tag{12}$$

where m_{p} is the particle mass, u_{f_i} is the continuous-phase velocity vector, u_{p_i} is the particle velocity vector, and g_i is the gravity vector. This equation assumes that the particle density is significantly greater than the fluid density so that other forces, such as the lift, the stress gradient, and the Basset history forces are negligible. Additionally, (12) employs a Stokesian drag to allow understanding of the fluid physics without introducing

the non-linearity and empiricism associated with high Reynolds number expressions. Including the particle relaxation time of (2) into (12) results in

$$\frac{\mathrm{d}u_{\mathrm{p}_i}}{\mathrm{d}t} = \frac{u_{\mathrm{f}_i} - u_{\mathrm{p}_i}}{\tau_{\mathrm{p}}} + g_i. \tag{13}$$

The non-dimensional equation of motion utilizing τ_{p} as the reference time scale and $u'_{\mathrm{f,rms}}$ as the reference velocity scale is integrated by both the DNS and CRW simulations using a modified version of the exponential-Lagrangian method first described by Barton (1996) and later generalized and improved by Bocksell (2004). This method is an Adams–Bashforth multistep integration scheme, implemented in a predictor–corrector fashion that is second-order accurate in time.

The particles are injected at every time step at $x = \Lambda_x/3$ and $y^+ = 4$ evenly distributed over the z-direction (50 spanwise locations as shown in Fig. 3). An elastic reflection is imposed at $y^+ = 1$ for all downstream wall interactions. The time step used for the DNS (both fluid and particle simulations) was constant for all cases and appears in Table 1 in various non-dimensional forms. The particle paths are computed and statistical information is recorded along the trajectories and fluxes (see Bocksell (2004) for relative particle concentration profiles) at various downstream planes until the last downstream plane, which is 15 boundary layer thicknesses from the injection location ($x = \Lambda_x/3 + 15\delta$). In order to understand how inertia influences particle diffusion in a boundary layer, five different particle inertias were selected with Stokes number varying from $St_\delta = 10^{-4}$ to $St_\delta = 1$, all at a constant γ of 10^{-2} (with V_{term} directed away from the wall). The low value of γ ensures that the terminal velocity is small compared to the fluid velocity fluctuations so that inertia and turbulent diffusion effects dominate the particle dispersion (as opposed to gravity). The conditions for the non-tracer particle simulations are also shown in Table 1 in terms of inner Stokes number (St^+) and outer Stokes number (St_δ). Since the time-scale of the turbulence varies with distance from the wall, the effective instantaneous Stokes number

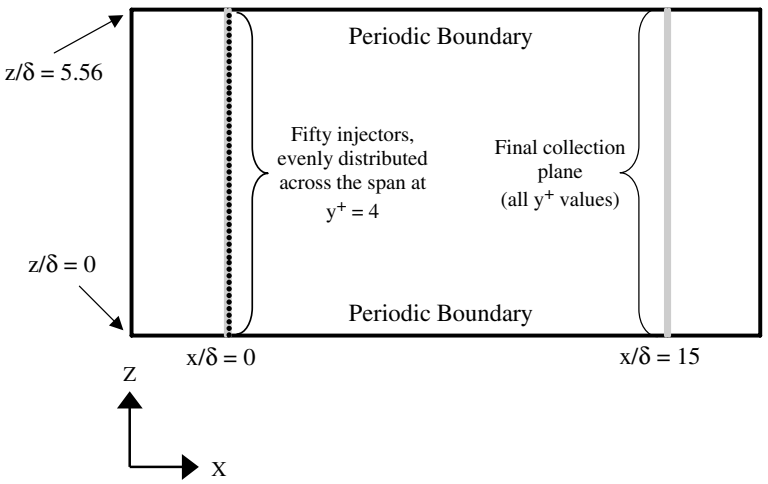

Fig. 3. Illustration of the particle injection locations as well as the particle tracking domain for the DNS. Note that there are five intermediate collection planes ($x/\delta = 0.5$, 1, 2, 4, 8).

Table 1
Particle conditions for the DNS particle simulations

St_δ	$\langle St_\Lambda \rangle$	St^+	$\frac{\Delta t}{\tau_{\mathrm{p}}}$	$\frac{\Delta t}{\tau^+}$	$\frac{\Delta t}{\tau_\delta}$
10^{-4}	7.8×10^{-4}	0.027	6.6×10^{-2}	0.57	0.0011
10^{-3}	7.8×10^{-3}	0.27	6.6×10^{-3}	0.57	0.0011
10^{-2}	8.3×10^{-2}	2.7	6.6×10^{-4}	0.57	0.0011
0.1	1.2	27	6.6×10^{-5}	0.57	0.0011
1	13.9	270	6.6×10^{-6}	0.57	0.0011

will vary depending on the particle location. By recording the observed integral fluid Lagrangian time scale (τ_Λ) along the particle path, an average local particle Stokes number was obtained, $\langle St_\Lambda \rangle = \tau_p / \langle \tau_\Lambda \rangle$, for each class of particles. As expected, the local Stokes number is bounded by St_δ and St^+, but tends to be closer to St_δ for the smallest particles. This is consistent with the result that the smallest particles diffuse the farthest away from the wall (as will be shown) where the outer Stokes number tends to govern the particle dynamics.

The DNS results are summarized in Fig. 5 in terms of the outer Stokes number and plotted a semi-log scale for y^+ to highlight the near-wall aspects. Fig. 4a–c show bullet plots of tracer particles ($St_\Lambda = 10^{-4}$ and $\gamma = 10^{-2}$) at three downstream locations ($x/\delta = 1$, 4, and 15), where each dot represents a distinct tracer particle's location as it crossed each x-plane. From the bullet plot at the $x/\delta = 1$ plane (Fig. 4a), the spatial coherency of the turbulence is evident as the particles are dispersed by the large-scale structures of the boundary layer yielding regions of high concentration associated with specific boundary layer ejection events. As the particles travel further downstream, this coherence disappears so that at $x/\delta = 15$ (Fig. 4c), there is little (if any) structure present in the bullet plot indicating that this downstream location is sufficient to provide fully

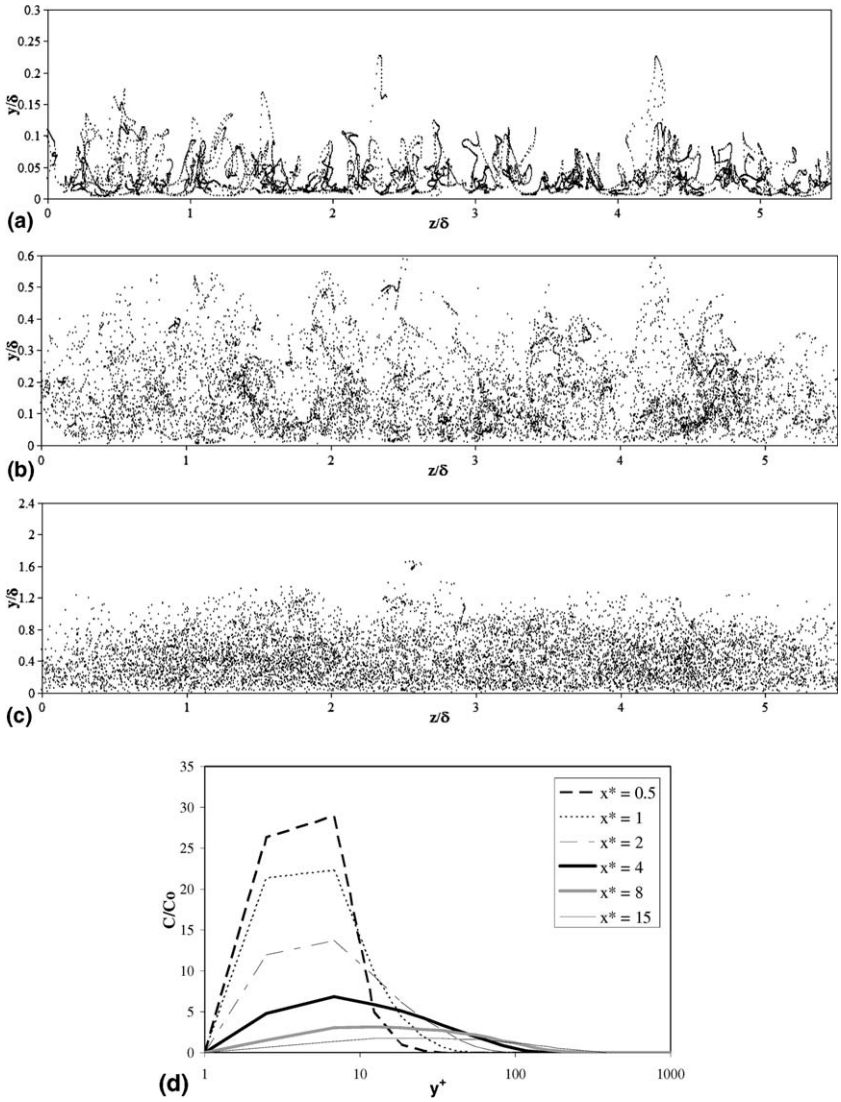

Fig. 4. Bullet plot of fluid-tracers ($St = 0$) at three downstream locations from DNS: (a) $x/\delta = 1$, (b) $x/\delta = 4$, (c) $x/\delta = 15$ along with (d) the resulting concentration profile.

diffuse conditions. Fig. 4d shows the resulting averaged particle concentration profiles for in wall units at this location, where it can be seen that the initial near-wall concentration is successively transported from the wall by turbulent diffusion. Further details of the particle dispersion physics are given in Dorgan (2003).

2.3. Investigated CRW methods

One of the main goals of this research is to evaluate the performance of the CRW model with regard to the amount of turbulence information available for successively increasing fluid physics information. Therefore, conventional and normalized Markov chains are described here for three different types of simulations: (1) isotropic turbulence, (2) anisotropic turbulence but no Reynolds stress, and (3) anisotropic turbulence with Reynolds stresses. For consistency, the time-scale treatment, the velocity fluctuation treatment, and the incremental drift correction treatment were all identical in terms of the level of turbulence information resulting in three types of CRW simulations to evaluate the importance of the anisotropy. These three simulation types are summarized in Table 2. Note that the CRW time-step for the particle trajectories was 3.3 times larger than the DNS time-step, which was sufficient for the presented statistical properties.

The conventional and normalized one-dimensional Markov chains for isotropic turbulence were presented in (4) and (6). The diagonal CRW models that utilize only the diagonal of the Reynolds stress tensor (σ_u, σ_v, and σ_w) are (conventional):

$$u_i(t+\Delta t) = \delta_{ijk} u_j(t) \exp\left(\frac{-\Delta t}{\tau_{\mathrm{L}_k}}\right) + \left[1 - \exp\left(\frac{-2\Delta t}{\tau_{\mathrm{L}_k}}\right)\right]^{1/2} \delta_{ijkl} \sigma_{\mathrm{u}_j}(t) \xi_l(t) \tag{14}$$

and similarly the normalized Markov chain is

$$u_i(t+\Delta t) = \delta_{ijklm} u_j(t) \exp\left(\frac{-\Delta t}{\tau_{\mathrm{L}_k}}\right) \frac{\sigma^*_{\mathrm{u}_l}(t+\Delta t)}{\sigma_{u_m}(t)} + \left[1 - \exp\left(\frac{-2\Delta t}{\tau_{\mathrm{L}_k}}\right)\right]^{1/2} \delta_{ijkl} \sigma^*_{\mathrm{u}_j}(t+\Delta t) \xi_l(t). \tag{15}$$

Considering the full Reynolds stress with the boundary layer approximations results in only the u–v cross-correlations as non-zero. Thus the resulting form for the conventional Markov chain for the "full" simulations is

$$\begin{bmatrix} u(t+\Delta t) \\ v(t+\Delta t) \\ w(t+\Delta t) \end{bmatrix} = \begin{bmatrix} k_u & 0 & 0 \\ 0 & k_v & 0 \\ 0 & 0 & k_w \end{bmatrix} \begin{bmatrix} u(t) \\ v(t) \\ w(t) \end{bmatrix} + \begin{bmatrix} \sigma_u\sqrt{1-k_u^2} & 0 & 0 \\ 0 & \sigma_v\sqrt{1-k_v^2} & 0 \\ 0 & 0 & \sigma_w\sqrt{1-k_w^2} \end{bmatrix} \begin{bmatrix} \sqrt{1-b^2} & b & 0 \\ 0 & 1 & 0 \\ 0 & 0 & 1 \end{bmatrix} \begin{bmatrix} \xi_u \\ \xi_v \\ \xi_w \end{bmatrix}, \tag{16}$$

where

$$k_u = \exp\left(\frac{-\Delta t}{\tau_{\mathrm{L}_u}}\right), \quad k_v = \exp\left(\frac{-\Delta t}{\tau_{\mathrm{L}_v}}\right), \quad k_w = \exp\left(\frac{-\Delta t}{\tau_{\mathrm{L}_w}}\right),$$
$$b = \frac{R_{uv}\left[1 - \exp\left(\frac{-\Delta t}{\tau_{\mathrm{L}_u}}\right)\exp\left(\frac{-\Delta t}{\tau_{\mathrm{L}_v}}\right)\right]}{\left[1 - \exp\left(\frac{-2\Delta t}{\tau_{\mathrm{L}_u}}\right)\right]^{1/2}\left[1 - \exp\left(\frac{-2\Delta t}{\tau_{\mathrm{L}_v}}\right)\right]^{1/2}}, \quad \text{and} \quad R_{uv} = \frac{\overline{uv}}{\sigma_u \sigma_v}. \tag{17}$$

Table 2
Summary of types of CRW simulations

Name	Turbulence type	Time-scale type
Isotropic	$\overline{uu} = \overline{vv} = \overline{ww} = 2K/3, \overline{uv} = 0$	$\tau_{\mathrm{L}_u} = \tau_{\mathrm{L}_v} = \tau_{\mathrm{L}_w}$
Diagonal	$\overline{uu} \neq \overline{vv} \neq \overline{ww}, \overline{uv} = 0$	$\tau_{\mathrm{L}_u} \neq \tau_{\mathrm{L}_v} \neq \tau_{\mathrm{L}_w}$
Full	$\overline{uu} \neq \overline{vv} \neq \overline{ww}, \overline{uv} \neq 0$	$\tau_{\mathrm{L}_u} \neq \tau_{\mathrm{L}_v} \neq \tau_{\mathrm{L}_w}$

The resulting normalized Markov chain for the "full" simulations is

$$\begin{bmatrix} u(t+\Delta t) \\ v(t+\Delta t) \\ w(t+\Delta t) \end{bmatrix} = \begin{bmatrix} k_u & 0 & 0 \\ 0 & k_v & 0 \\ 0 & 0 & k_w \end{bmatrix} \begin{bmatrix} \frac{\sigma_u^*(t+\Delta t)}{\sigma_u(t)} & 0 & 0 \\ 0 & \frac{\sigma_v^*(t+\Delta t)}{\sigma_v(t)} & 0 \\ 0 & 0 & \frac{\sigma_w^*(t+\Delta t)}{\sigma_w(t)} \end{bmatrix} \begin{bmatrix} u(t) \\ v(t) \\ w(t) \end{bmatrix} + \begin{bmatrix} \sigma_u^*(t+\Delta t)\sqrt{1-k_u^2} & 0 & 0 \\ 0 & \sigma_v^*(t+\Delta t)\sqrt{1-k_v^2} & 0 \\ 0 & 0 & \sigma_w^*(t+\Delta t)\sqrt{1-k_w^2} \end{bmatrix} \times \begin{bmatrix} \sqrt{1-b^2} & b & 0 \\ 0 & 1 & 0 \\ 0 & 0 & 1 \end{bmatrix} \begin{bmatrix} \xi_u \\ \xi_v \\ \xi_w \end{bmatrix}, \tag{18}$$

where k_u, k_v, k_w, b and R_{uv} are the same as (17). The main difference between the conventional Markov chain of (16) and the normalized Markov chain of (18) is the ratio of the root-mean-square of the velocity fluctuations from the last time step and the next time step. Essentially this provides decorrelation in the time history of the velocity fluctuation where gradients in the turbulence are large (near the wall). It is also noteworthy that Mito and Hanratty (2005) utilize an anisotropic formulation of the Langevin equation that provides higher order statistical information and fidelity.

2.4. Particle drift correction for finite-inertia particles

As noted in the introduction, a finite mass particle drift correction for both the conventional and normalized Markov chains has been developed in this study. This correction is different than previous fluid-tracer drift corrections since the total differential of the fluid velocity fluctuation along a particle trajectory includes both the fluid and particle velocity fluctuations:

$$\frac{\mathrm{d}u'_{\mathrm{f}_i}}{\mathrm{d}t} = \frac{\partial u'_{\mathrm{f}_i}}{\partial t} + u_{\mathrm{p}_j}\frac{\partial u'_{\mathrm{f}_i}}{\partial x_j}. \tag{19}$$

Taking the Eulerian time-average results in

$$\overline{\frac{\mathrm{d}u'_{\mathrm{f}_i}}{\mathrm{d}t}} = \overline{u_{\mathrm{p}_j}\frac{\partial u'_{\mathrm{f}_i}}{\partial x_j}}. \tag{20}$$

The goal is to estimate the right-hand-side correlation between the particle velocity and fluid fluctuation velocity with particle characteristics and Eulerian fluid correlations. Starting with the particle equation of motion (13) and introducing Reynolds averaging ($u_{\mathrm{f}_i} = \overline{u_{\mathrm{f}_i}} + u'_{\mathrm{f}_i}$), results in

$$\frac{\mathrm{d}u_{\mathrm{p}_i}}{\mathrm{d}t} + \frac{u_{\mathrm{p}_i}}{\tau_{\mathrm{p}}} = \frac{u'_{\mathrm{f}_i}}{\tau_{\mathrm{p}}} + \left(\frac{\overline{u_{\mathrm{f}_i}}}{\tau_{\mathrm{p}}} + g_i\right). \tag{21}$$

Utilizing Laplace transforms, (21) becomes

$$u_{\mathrm{p}_i}(s)\left(s + \frac{1}{\tau_{\mathrm{p}}}\right) = u_{\mathrm{p}_i}(0) + \frac{1}{\tau_{\mathrm{p}}}u'_{\mathrm{f}_i}(s) + \frac{1}{s}\left(\frac{\overline{u_{\mathrm{f}_i}}}{\tau_{\mathrm{p}}} + g_i\right), \tag{22}$$

where £ denotes the Laplace transform so that $u_{\mathrm{p}_i}(s) = £[u_{\mathrm{p}_i}(t)]$ and $u'_{\mathrm{f}_i}(s) = £[u'_{\mathrm{f}_i}(t)]$.

Inversion results in the solution to the particle equation of motion in the time domain as

$$u_{\mathrm{p}_i}(t) = u_{\mathrm{p}_i}(0)\exp\left(\frac{-t}{\tau_{\mathrm{p}}}\right) + \frac{1}{\tau_{\mathrm{p}}}\int_0^t \exp\left(\frac{r-t}{\tau_{\mathrm{p}}}\right)u'_{\mathrm{f}_i}(r)\,\mathrm{d}r + \left(\overline{u_{\mathrm{f}_i}} + \tau_{\mathrm{p}}g_i\right)\left[1 - \exp\left(\frac{-t}{\tau_{\mathrm{p}}}\right)\right]. \tag{23}$$

The correlation of interest, $\overline{u_{\mathrm{p}_j}\partial u'_{\mathrm{f}_i}/\partial x_j}$, is obtained from multiplying (23) by $\partial u'_{\mathrm{f}_i}/\partial x_j$ and time-averaging (noting that $\overline{\partial u'_{\mathrm{f}_i}/\partial x_j} = 0$ and $\overline{\xi(t)\partial u'_{\mathrm{f}_i}/\partial x_j} = 0$) which results in

$$\overline{u_{\mathrm{p}_j}(t)\frac{\partial u'_{\mathrm{f}_i}(t)}{\partial x_j}} = \overline{u_{\mathrm{p}_j}(0)\frac{\partial u'_{\mathrm{f}_i}(t)}{\partial x_j}}\exp\left(\frac{-t}{\tau_{\mathrm{p}}}\right) + \frac{1}{\tau_{\mathrm{p}}}\int_0^t \exp\left(\frac{r-t}{\tau_{\mathrm{p}}}\right)\overline{u'_{\mathrm{f}_j}(r)\frac{\partial u'_{\mathrm{f}_i}(t)}{\partial x_j}}\mathrm{d}r. \tag{24}$$

The correlation of $\overline{u'_{\mathrm{f}_j}(s)\partial u'_{\mathrm{f}_i}(t)/\partial x_j}$ appearing in the above equation is simplified for locally homogeneous turbulence by assuming a standard decorrelation form of

$$\overline{u'_{\mathrm{f}_j}(s)\frac{\partial u'_{\mathrm{f}_i}(t)}{\partial x_j}} = \overline{u'_{\mathrm{f}_j}(t)\frac{\partial u'_{\mathrm{f}_i}(t)}{\partial x_j}}\exp\left(\frac{s-t}{\tau_{\Lambda}}\right). \tag{25}$$

Substituting (25) into (24) and then integrating for the limit $t \to \infty$, as discussed by Bocksell (2004), results in the "finite-inertia incremental drift correction" as

$$\overline{u_{\mathrm{p}_j}\frac{\partial u'_{\mathrm{f}_i}}{\partial x_j}} = \overline{u'_{\mathrm{f}_j}\frac{\partial u'_{\mathrm{f}_i}}{\partial x_j}}\left(\frac{1}{1+St_{\Lambda}}\right). \tag{26}$$

This finite-inertia drift correction tends to the proper fluid-tracer correction (8) as the particle inertia becomes negligible ($St_{\Lambda} \to 0$), while it tends to zero as the particle inertia becomes high ($St_{\Lambda} \gg 0$). This latter limit is consistent with the eventual elimination of the correlation between fluid and particle velocity fluctuations for very large particles. Note that these limits would be observed even if a non-linear drag coefficient were used such that (26) is expected to be at least qualitatively reasonable at high particle Reynolds numbers.

The finite-inertia drift correction for the normalized Markov chain is similarly obtained for the normalized Langevin equation. The total differential of the normalized variable utilized in the normalized Langevin equation along a finite inertia particle is

$$\overline{\frac{\mathrm{d}}{\mathrm{d}t}\left(\frac{u'_{\mathrm{f}_k}}{\sigma_{\mathrm{u}_l}}\right)\delta_{ikl}} = \overline{u_{\mathrm{p}_j}\frac{\partial}{\partial x_j}\left(\frac{u'_{\mathrm{f}_k}}{\sigma_{\mathrm{u}_l}}\right)\delta_{ikl}}. \tag{27}$$

Note that the term $(u'_{\mathrm{f}_k}/\sigma_{\mathrm{u}_l})\delta_{ikl}$, could be re-written as $(u'_{\mathrm{f}_i}/\sigma_{\mathrm{u}_i})$ if there is *no* summation over the "i" index. This equation is multiplied by $\partial(u'_{\mathrm{f}_k}/\sigma_{\mathrm{u}_l})/\partial x_j\delta_{ikl}$, and after Laplace transformation analysis performed by Bocksell (2004), the corresponding finite-inertia incremental drift correction is

$$\overline{u_{\mathrm{p}_j}\frac{\partial}{\partial x_j}\left(\frac{u'_{\mathrm{f}_k}}{\sigma_{\mathrm{u}_l}}\right)\delta_{ikl}} = \overline{u'_{\mathrm{f}_j}\frac{\partial}{\partial x_j}\left(\frac{u'_{\mathrm{f}_k}}{\sigma_{\mathrm{u}_l}}\right)\delta_{ikl}}\left(\frac{1}{1+St_{\Lambda}}\right). \tag{28}$$

Thus, for both the conventional and normalized Markov chains, the factor used to transform the particle–fluid correlation to fluid–fluid correlations, $1/(1+St_{\Lambda})$, is identical such that the same limits occur.

When implementing the incremental drift correction for the CRW simulations, the turbulence correlations for the drift correction are treated in a consistent manner as for the rest of the Markov chain. For example, if the time and length scales for the CRW simulation are assumed isotropic, then the turbulence correlations in the incremental drift correction are also assumed isotropic (various forms of the tested CRW models are given in Table 3). Next, the DNS results are presented to describe the basic turbulent diffusion features followed by the CRW results where the various formulations are compared to the DNS statistics.

Table 3
Summary of the types of incremental drift velocities utilized for the CRW model

Drift type	Markov chain	Increment drift formula
No drift	Conventional and normalized	$\overline{\delta u'_{\mathrm{f}_i}} = 0$
Fluid-tracer	Conventional	$\overline{\delta u'_{\mathrm{f}_i}} = \Delta t\overline{u'_{\mathrm{f}_j}\frac{\partial u'_{\mathrm{f}_i}}{\partial x_j}}$
Finite-inertia	Conventional	$\overline{\delta u'_{\mathrm{f}_i}} = \Delta t\overline{u'_{\mathrm{f}_j}\frac{\partial u'_{\mathrm{f}_i}}{\partial x_j}}\left(\frac{1}{1+St}\right)$
Fluid-tracer	Normalized	$\overline{\delta u'_{\mathrm{f}_i}} = \Delta t\overline{u'_{\mathrm{f}_j}\frac{\partial u}{\partial x_j}\left(\frac{u'_{\mathrm{f}_k}}{\sigma_{\mathrm{u}_l}}\right)}\delta_{ikl}$
Finite-inertia	Normalized	$\overline{\delta u'_{\mathrm{f}_i}} = \Delta t\overline{u'_{\mathrm{f}_j}\frac{\partial u}{\partial x_j}\left(\frac{u'_{\mathrm{f}_k}}{\sigma_{\mathrm{u}_l}}\right)}\delta_{ikl}\left(\frac{1}{1+St}\right)$

3. CRW results

3.1. Transverse concentration profiles

To test the drift corrections, fluid-tracer particles ($m_p \sim 0$, $St_\delta \sim 0$) were injected throughout the boundary layer (from $y = 0$ to $y > \delta$) and by conservation of mass, the concentration profile should remain uniform as they move downstream (in an averaged sense). Fig. 5a shows the results of the CRW simulations of this type of tracer particle injection with isotropic turbulence and isotropic time scale using the conventional Markov chain of (4). The ideal result is a uniform concentration as shown by the solid line, but there is a significant

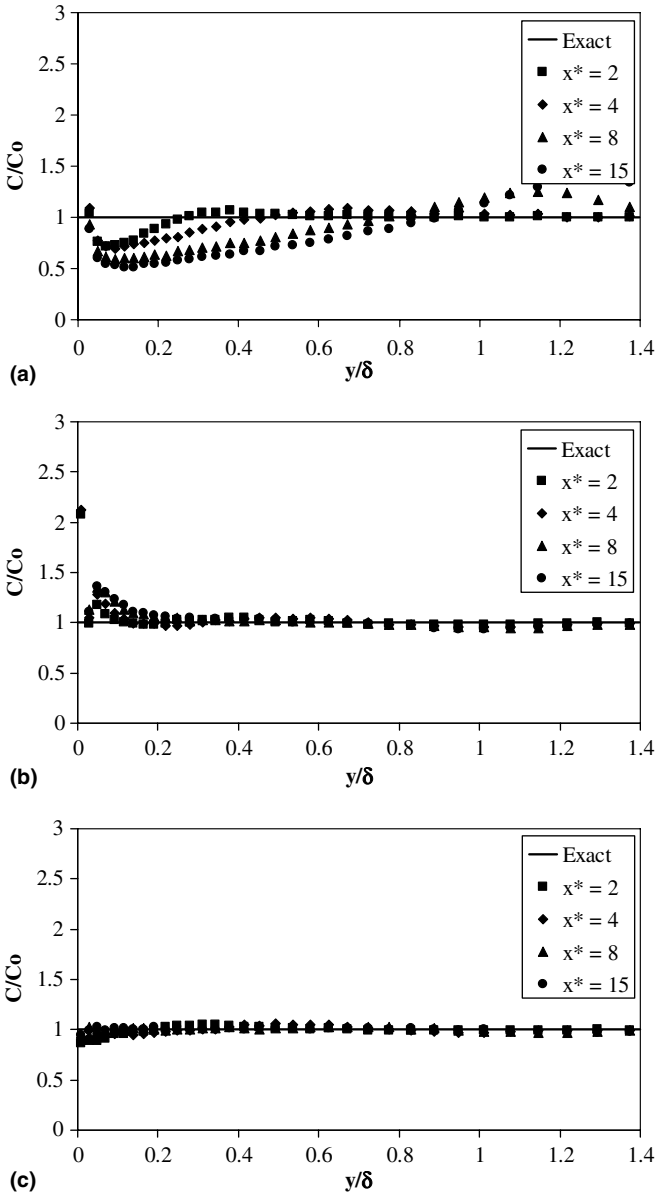

Fig. 5. Fluid-tracer particle concentration profiles for the turbulent boundary layer (injected uniformly at $x^* = 0$, or $x/\delta = 0$) at four downstream locations for the CRW model with: (a) conventional Markov chain with no drift correction, (b) conventional Markov chain with conventional tracer drift correction, (c) modified Markov chain with modified tracer drift correction.

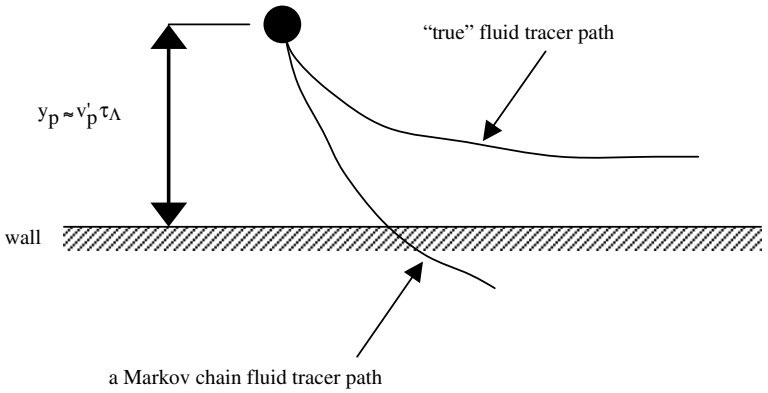

Fig. 6. Schematic illustrating the history effect of the conventional Markov chain near the wall that results in a non-physical wall collision compared to the true fluid particle path with a more rapid decorrelation (due to the presence of the wall).

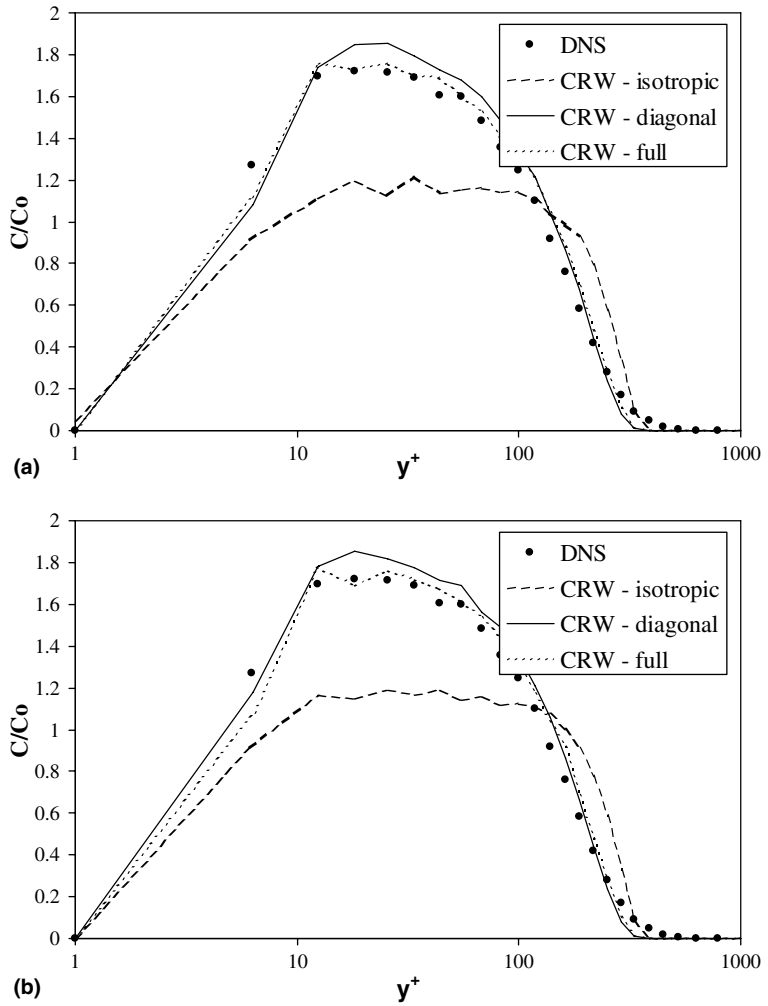

Fig. 7. Comparison of particle concentration profiles from DNS and CRW simulations for $St_\delta = 10^{-4}$ at $x/\delta = 15$ for with (a) fluid-tracer incremental drift correction and (b) finite-inertia incremental drift correction.

amount of wall-peaking such that the particle concentrations at the first point are off the chart ($C/C_o > 4.5$). Including the incremental drift correction for the conventional, isotropic Markov chain (see Table 3) substantially reduces the non-physical peaks of particle concentration in the outer region of the boundary layer as shown in Fig. 5b, but there is still significant wall-peaking ($C/C_o > 2.0$). This case also yielded a high number of non-physical wall collisions for the fluid-tracer particles (about 50 collisions for every 1000 particle injected). Thus, there is an incorrect description of the CRW velocity perturbations for tracer trajectories as particles approach the wall. To understand the genesis of the problem, consider the conventional Markov chain (4). The fluctuation velocity at the next time step is based on the value of the fluctuation velocity at the previous time step, and this "history" effect will influence the fluctuation value for a time duration of approximately τ_A. However, for fluid-tracer particles moving towards the wall, conditions can arise so that this history effect non-physically drives the fluid particle into the wall and a collision results. A true fluid particle should never bounce because of the wall boundary condition ($\overline{v_f} = 0$) and the Eulerian velocity fluctuation ($v'_{f_{rms}}$) approaches zero (quadratically) at the wall (see Fig. 1c). To see how this problem can readily occur for the conventional Markov chain, consider a fluid particle approaching the wall and having a negative (wall-ward) transverse velocity fluctuation such that $|v'_f(t)| > \tau_{int}/y_p$, as shown in Fig. 6. This situation is reasonable since $v'_{f_{rms}}$ is on the order of τ_A/y for $10 < y^+ < 20$ (Fig. 1c). In this case, there is a high probability that

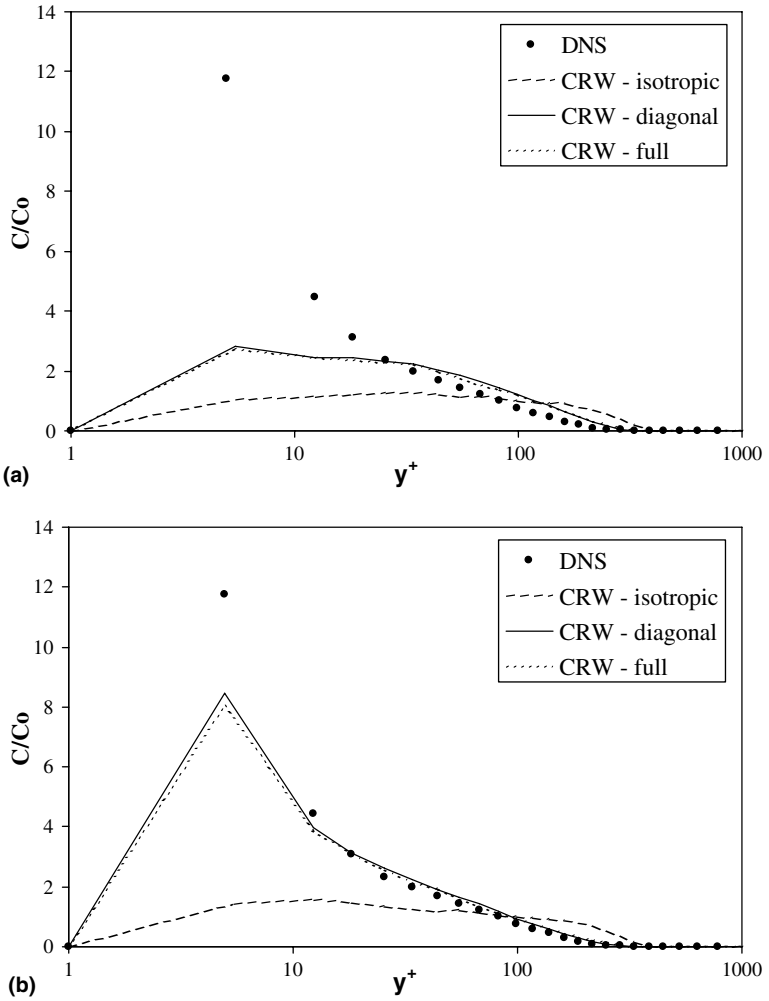

Fig. 8. Comparison of particle concentration profiles from DNS and CRW simulations for $St_\delta = 10^{-1}$ at $x/\delta = 15$ for with (a) fluid-tracer incremental drift correction and (b) finite-inertia incremental drift correction.

the fluid-tracer particle will improperly collide since the conventional Markov chain decorrelation rate will generally be insufficient to reduce $v'_f(t)$ to zero before the particle arrives at the wall, and thus a large number of non-physical collisions are recorded for tracer particles. This problem is rectified by using the normalized Markov chain, as discussed below.

The normalized, isotropic Markov chain (6) is constructed from the normalized Langevin equation of (5), which is simply a transformation from inhomogeneous turbulence to homogenous turbulence. It provides a better model for the decorrelation as a particle moves from a region of high turbulence to a region of low turbulence due to the presence of the ratio, $\sigma(t+\Delta t)/\sigma(t)$, in (6). Application of this normalized Markov chain yielded an order of magnitude reduction in wall collisions. This improvement is also reflected in Fig. 5c, which shows the concentration profiles and it is evident that the CRW results are close to the exact solution throughout the boundary layer. Because of this, all the CRW simulations shown hereafter utilize the normalized Markov chain. Results utilizing the conventional Markov chain are given in Bocksell (2004).

Fig. 7 contains the results for the $St_\delta = 10^{-4}$ particles at the last collection plane, $x/\delta = 15$, such that $t \gg \tau_\Lambda$ for the fluid-tracer and finite-inertia drift corrections. In Fig. 7a, the concentration profiles from the diagonal and full Reynolds-stress CRW simulations are quite close to the results from the DNS, where the full Reynolds-stress results are slightly better. However, the simulations utilizing the isotropic normalized Markov

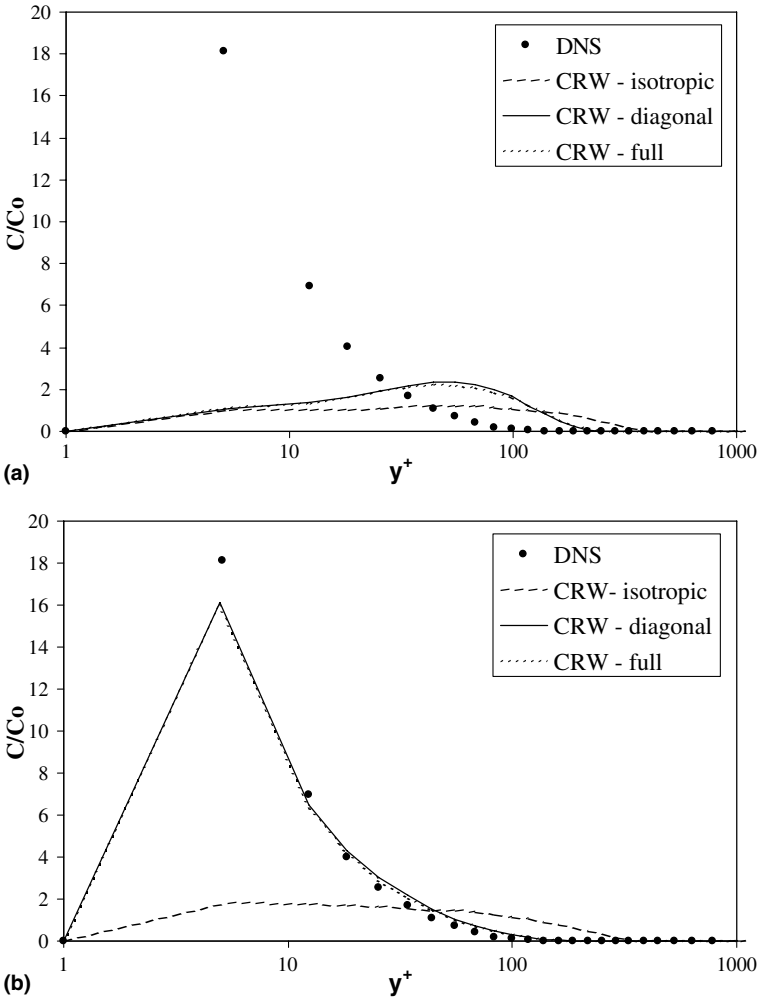

Fig. 9. Comparison of particle concentration profiles from DNS and CRW simulations for $St_\delta = 1$ at $x/\delta = 15$ for with (a) fluid-tracer incremental drift correction and (b) finite-inertia incremental drift correction.

chain significantly under predict the particle diffusion in the $10 < y^+ < 100$ region. This is reasonable since the isotropic definition of the transverse velocity fluctuations from the kinetic energy results in an over-estimate of the actual $v'_{f_{rms}}$ values (Fig. 1c) and thus causes the particles to diffuse faster way from the wall and reduces the near-wall concentration. These results indicate that anisotropy in a boundary layer should be included in the Markov chain to obtain accurate near-wall results. Fig. 7b shows the same results (as expected) since the particle Stokes number is very small and the differences between the fluid-tracer and finite-inertia drift corrections are negligible.

Fig. 8 shows the downstream concentration profiles for particles with $St_\delta = 10^{-1}$. As the particle inertia increases, the diffusion away from the wall is lessened so the peak (near-wall) particle concentration is increased. In Fig. 8a the CRW simulations with the fluid-tracer drift correction significantly under-predict the concentration profile near the wall especially at the peak concentration location compared to the DNS. Including the finite-inertia drift correction (see Fig. 8b) dramatically improves the agreement of the CRW simulations with the tracer drift correction to the DNS results, although there is still a slight under prediction near the wall at the peak location. This indicates the importance of the finite-inertia effects on the drift correction for local particle Stokes numbers of order unity. A significant improvement (though not as dramatic) is also seen for $St_\delta = 10^{-2}$ by Bocksell (2004), which is somewhat surprising given that its effective Stokes number is on the order of 10^{-1}. For both $St_\delta = 10^{-2}$ and $St_\delta = 10^{-1}$, the improvement with an anisotropic turbulence model is substantial but the improvement with adding the off-diagonal terms is slight. The results for particles with the largest Stokes number ($St_\delta = 1$) appear in Fig. 9 and show the same trends but with even more importance of the finite-inertia drift correction. Results for other streamwise locations for the full range of particle Stokes numbers exhibited the same features as discussed by Bocksell (2004).

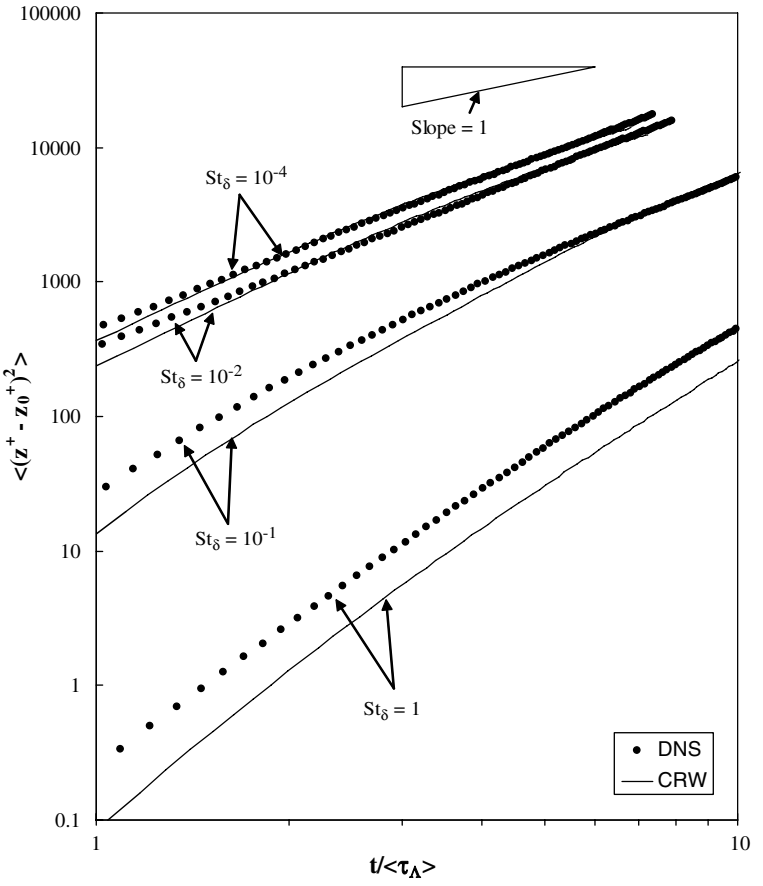

Fig. 10. Mean-square particle position in the spanwise direction (z) for various Stokes numbers showing both DNS and CRW results.

3.2. Mean-square particle position

Another area of investigation was the root-mean-square of the particle location (in spanwise and transverse directions) as a function of time. To examine the prediction of this positional variance, the best performing technique (normalized CRW with an anisotropic diagonal and finite-inertia drift correction) was employed as a "baseline" model. Spanwise diffusion is considered first since effects of inhomogeneous flow are only indirect (there are no spanwise gradients in the mean and turbulence statistics). Fig. 10 shows a comparison of the mean-square spanwise (z) diffusion of the "baseline" CRW simulations to the DNS. The mean-square diffusion for $St_\delta = 10^{-4}$ and $St_\delta = 10^{-2}$ closely match the DNS results, especially for long times $t \gg \tau_\Lambda$, where the slopes approach unity, consistent with long time tracer particle diffusion in HIsT. For particles with $St_\delta = 10^{-1}$, the average positional root-mean-square is significantly reduced due to inertia effects (as compared to the smaller Stokes number cases), but the agreement between the CRW and DNS is still reasonable, especially at long times. The $St_\delta = 1$ case yields strongly reduced spanwise diffusion even far downstream due both to the increased inertia and the fact that the particles remain near the wall (Fig. 9b) and thus are exposed to a much reduced $w'_{f_{rms}}$ (Fig. 1c). This result is at least qualitatively found for both the DNS and CRW results (the differences between DNS and CRW for this case are somewhat exaggerated due to the use of a log–log plot). It should also be noted that the DNS diffusion rate (slope of these curves) is super-quadratic for this case and this is not predicted by short-time HIsT theory, yet it is reasonably predicted with the CRW results.

Fig. 11 shows a comparison of the mean-square wall-normal (y) diffusion for the "baseline" CRW simulations to the DNS results. In general, the initial wall-normal diffusion (CRW and DNS) is an order of magnitude less than the spanwise diffusion for a given time which can be attributed to the fact that $v'_{f_{rms}}$ is much less

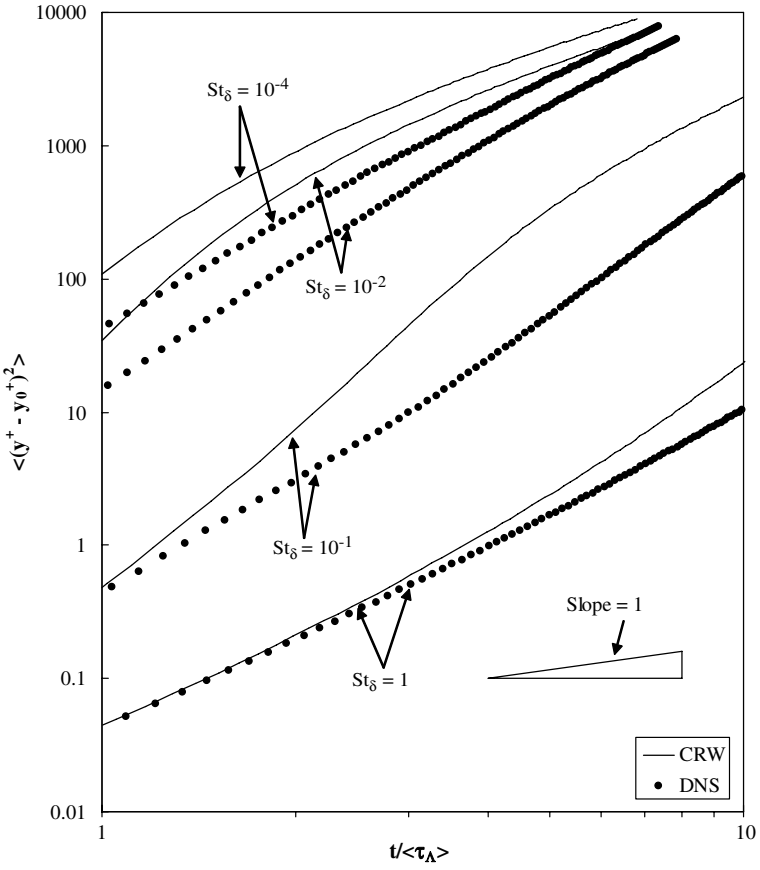

Fig. 11. Mean-square particle position in the wall-normal direction (y) for various Stokes numbers showing both DNS and CRW results.

than $w'_{f_{rms}}$ near the wall (Fig. 1c). However, the transverse diffusion exhibits much steeper curves, e.g., super-quadratic at even the longest-time periods. These mean diffusion root-mean-square values and the effective slopes are qualitatively predicted by the CRW results but there are some significant differences. The CRW simulation for particles of $St_\delta = 1$ has the closest agreement to the DNS results, which is consistent with the results shown for the concentration profiles, though there is a tendency to over-predict diffusion at long times. For the other particle inertias, the CRW results tend to over-predict diffusion for intermediate times, which was consistent with the concentration profile comparisons at locations before x/δ of 15. The discrepancies may be due to insufficient drift correction especially when time-scales change drastically (Fig. 2) or the assumption of a single time and length scale of the turbulence in the buffer and near-wall regions where fundamental turbulent scales and physics differ substantially from the outer region. Another possible problem could be the assumption of a Gaussian distribution for the fluctuation velocities, since Iliopoulos and Hanratty (1999) showed that skewness and flatness (though typically not available for RANS flowfields) can improve CRW predictions.

Finally, in order to assess the mean particle trajectory movement due to turbulence, Fig. 12 shows a comparison of the time-averaged, wall-normal particle velocity averaged along the particle trajectory, $\langle v_p \rangle$, normalized by the terminal velocity, and plotted as a function of particle Stokes number. Since $\langle v_p \rangle$ is always

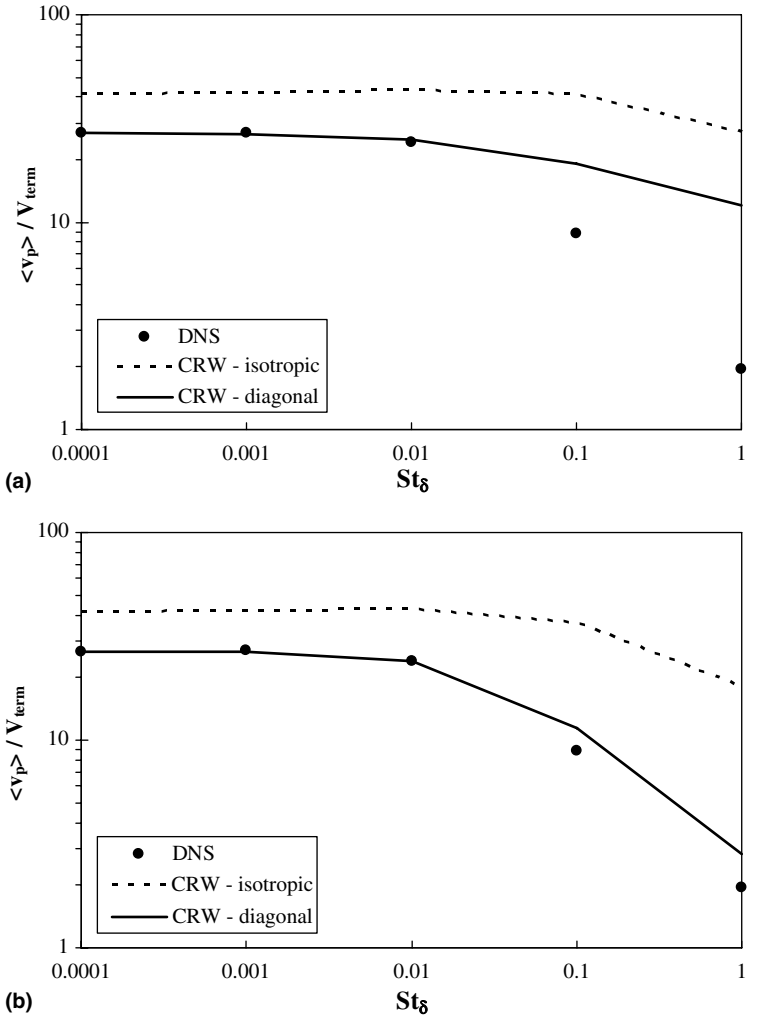

Fig. 12. Plot of the averaged vertical (wall-normal) particle velocity normalized by the terminal velocity versus particle Stokes numbers for (a) fluid-tracer particle incremental drift correction and (b) finite-inertia incremental drift correction.

greater than V_{term}, the net movement away from the wall is generally dominated by turbulent diffusion. This is especially true for the tracer-like particles ($St_\delta = 10^{-4}$) for which the velocity ratio is nearly 30. However, for the largest particles ($St_\delta = 1$) the mean transverse velocity approaches the terminal velocity condition. Fig. 12a contains the results from the CRW simulations with the tracer-particle drift correction and Fig. 12b contains the CRW simulations with the finite-inertia drift correction; both cases also compare the isotropic and anisotropic diagonal CRW models. In general, the anisotropic effect is important at all Stokes numbers while the isotropic model consistently over-predicts the mean transverse velocity. For the anisotropic CRW simulations, the fluid-tracer drift correction is reasonable up to $St_\delta = 10^{-2}$ ($St_\Lambda = 8.3 \times 10^{-2}$). However, for particles with $St_\delta = 10^{-1}$($St_\Lambda = 1.2$) and larger, the finite-inertia drift correction is needed and gives reasonable results.

4. Conclusions

Several CRW models were developed and tested for near-wall particle diffusion in a turbulent boundary layer. The CRW models were based on continuous-flow Eulerian statistics derived from the DNS solution combined with an instantaneous particle equation of motion. The integral-time scales of the continuous-phase turbulence were found to be approximately isotropic and were reasonably approximated by the model of Kallio and Reeks (1989). The particle test conditions included a variety of Stokes numbers varying from St^+ of 0.27–270, while the terminal velocity was kept small so that it did not significantly affect the mean movement of the particles. To assess the performance of the various models, the CRW results were compared to DNS particle diffusion statistics. Thus, the DNS and CRW particle trajectories were based on continuous-phase flows with the same Eulerian flow statistics. This consistency eliminated any differences associated with empiricism from turbulence modeling or uncertainties associated with experimental measurements.

The DNS concentration profiles indicated that the particle inertia strongly controlled the level of spanwise diffusion, as small particles diffused much more rapidly than large particles consistent with homogeneous diffusion theory. However, the wall-normal (transverse) diffusion was more complex and with large departures from that expected by homogeneous diffusion. Investigation of mass conservation with fluid-tracer particles indicated that a modified (non-dimensionalized) Markov chain was needed for the CRW model to prevent non-physical diffusion associated with large gradients in turbulence near the wall. In addition, an incremental drift correction for the Markov chain, which is a function of particle Stokes number, was critical to avoiding non-physical particle collection in low-turbulence regions for particle Stokes numbers (based on the local integral turbulence time scale) on the order of unity or more.

Various level of Eulerian statistics were also tested in terms of prediction of the transverse particle concentration profiles. It was found that inclusion of the full Reynolds stress tensor, especially variations in the diagonal elements, was important and yielded good comparison with the DNS results at a downstream location consistent with particles traveling for several integral turbulent time-scales. Therefore, the recommended model includes the anisotropic Eulerian turbulence statistics along with a normalized Markov chain and an finite-inertia drift correction. However, even this model was not able to predict some of the detailed near-wall particle root-mean-square statistics associated with transverse diffusion, suggesting that further improvement may require non-Gaussian statistics and/or incorporation of more detailed description of the near-wall variations in integral length- and time-scales.

Acknowledgements

The authors would like to acknowledge Dr. P. K. Yeung for help with obtaining the DNS continuous-phase results, Mr. A. Dorgan help with obtaining the DNS particle-phase results, the Defense Advanced Research Projects Agency (DARPA) for funding support, and MHPCC for computer allocation time.

Disclaimer: Any opinions, findings, and conclusions or recommendations expressed in this publication are those of the authors and do not necessarily reflect the views of DARPA.

References

Barton, I.E., 1996. Exponential-Lagrangian tracking schemes applied to Stokes law. J. Fluids Eng. 118, 85–89.

Bocksell, T.L., 2004. Numerical simulation of turbulent particle diffusion. Ph.D. Thesis, University of Illinois at Urbana-Champaign, Urbana, IL.

Bocksell, T.L., Loth, E., 2001. Random walk models for particle diffusion in free-shear flows. AIAA J. 39, 1086–1096.

Crowe, C.T., Chung, J.N., Troutt, T.R., 1988. Particle mixing in free shear flows. Prog. Energy Combust. Sci. 14, 171–194.

Dorgan, A.J., 2003. Boundary layer dispersion of near-wall injected particles of various inertias. M.S. Thesis, University of Illinois at Urbana-Champaign, Urbana, IL.

Hinze, J.O., 1975. Turbulence. McGraw-Hill, New York.

Iliopoulos, I., Hanratty, T.J., 1999. Turbulent dispersion in a non-homogeneous field. J. Fluid Mech. 392, 45–71.

Kaftori, D., Hetsroni, G., Banerjee, S., 1995. Particle behavior in the turbulent boundary layer II. Velocity and distribution profiles. Phys. Fluids 7, 1107–1121.

Kallio, G.A., Reeks, M.W., 1989. A numerical simulation of particle deposition in turbulent boundary layers. Int. J. Multiphase Flow 15, 433–446.

Legg, B.J., Raupach, M.R., 1982. Markov-chain simulation of particle dispersion in inhomogeneous flows: the mean drift correction induced by a gradient in the Eulerian velocity variance. Bound.-Layer Meteorol. 24, 3–13.

Loth, E., 2000. Numerical approaches for motion of dispersed particles, droplets, and bubbles. Prog. Energy Combust. Sci. 26, 161–223.

MacInnes, J.M., Bracco, F.V., 1992. Stochastic particle dispersion modeling and the tracer-particle limit. Phys. Fluids A 12, 2809–2824.

Mito, Y., Hanratty, T.J., 2005. A stochastic description of wall sources in a turbulent field. Part 3: effect of gravitational settling on the concentration profiles. Int. J. Multiphase Flow 31, 155–178.

Spalart, P.R., Watmuff, J.H., 1993. Experimental and numerical study of a turbulent boundary layer with pressure gradients. J. Fluid Mech. 249, 337–371.

Wilson, J.D., Thurtell, G.W., Kidd, G.E., 1981. Numerical simulation of particle trajectories in inhomogeneous turbulence. Part 2. Systems with variable turbulent velocity scale. Bound.-Layer Meteorol. 21, 423.

Young, J., Leeming, A., 1997. A theory of particle deposition in a turbulent pipe flow. J. Fluid Mech. 340, 129–159.